Magnetic-field tuning of the low-temperature state of $YbNiSi_3$

Sergey L. Bud'ko and Paul C. Canfield
Ames Laboratory U.S. DOE and Department of Physics and Astronomy, Iowa State University, Ames, Iowa 50011, USA

Marcos A. Avila and Toshiro Takabatake
Department of Quantum Matter, ADSM, Hiroshima University, Higashi-Hiroshima, Hiroshima 739-8530, Japan
(Received 12 December 2006; published 29 March 2007)

We present detailed data from low-temperature magnetization, magnetoresistance, and specific heat measurements on single-crystal $YbNiSi_3$ with the magnetic field applied along the easy magnetic axis, $H \| b$. An initially antiferromagnetic ground state changes into a field-stabilized metamagnetic phase at ~16 kOe ($T \to 0$). On further increase of the magnetic field, magnetic order is suppressed at ~85 kOe. No non-Fermi-liquid-like power law was observed in the resistivity in the vicinity of the critical field for $T \geqslant 0.4$ K. Heat capacity measurements suggest that the applied magnetic field splits the nearly degenerate crystal-electric-field levels that form the zero-field ground state of $YbNiSi_3$. The functional behaviors of the resistivity and specific heat are discussed in comparison with those of the few other stoichiometric heavy fermion compounds with established field-induced quantum critical points.

DOI: 10.1103/PhysRevB.75.094433 PACS number(s): 75.20.Hr, 72.15.Qm, 75.30.Kz

The "quantum criticality conundrum"[1] continues to be a focus of attention for many theorists and experimentalists.[2–8] In the particular case of magnetic intermetallic compounds that manifest heavy fermion ground states, magnetic ordering temperatures can be tuned by a variety of control parameters to $T=0$, bringing the material to a quantum critical point (QCP). This tuning is possible because of a delicate balance between the Ruderman-Kittel-Kasuya-Yoshida (RKKY) interaction, which defines the magnetic ordering temperature, and the Kondo effect, which causes screening of the magnetic moments and favors a nonmagnetic ground state.[9] Recently, in addition to traditionally used pressure and chemical substitution, magnetic field has also emerged as a potential control parameter,[2,6] having the advantages of being both a continuous and a common parameter for a number of experimental techniques. However, the applicability of a single theoretical description for a QCP reached by using different tuning parameters is still under discussion.

So far, the number of *stoichiometric* materials exhibiting a field-induced QCP is rather small, with only few of them being Yb based: $YbRh_2Si_2$,[10] YbAgGe,[11] and YbPtIn.[12] The release of entropy associated with the magnetic ordering (which can be used as a rough caliper of the size of the Yb magnetic moment in the ordered state) in the three materials ranges from $\sim 0.01R \ln 2$ for $YbRh_2Si_2$ to $\leqslant 0.1R \ln 2$ for YbAgGe to $\sim 0.6R \ln 2$ for YbPtIn. Nevertheless, the H-T phase diagrams and functional behavior of a number of physical parameters in the vicinity of the field-induced QCP are very similar for all three of these compounds. Recently investigated $YbNiSi_3$,[13] an orthorhombic, moderately heavy fermion compound with the Néel temperature, $T_N=5.1$ K, Sommerfeld coefficient, $\gamma \approx 190$ mJ/mol K^2, and entropy associated with the magnetic ordering, $\sim 0.6R \ln 2$, seems to be a suitable candidate for further studies of field-induced quantum criticality in stoichiometric Yb-based compounds.

Single crystals of $YbNiSi_3$ were grown from Sn flux (see Ref. 13 for more details). Residual flux from the surface of the samples was polished and/or etched off so as to exclude the effect of elemental Sn on measured electrical transport properties. dc magnetization was measured up to 55 kOe and down to 1.8 K in a Quantum Design MPMS-5 superconducting quantum interference device (SQUID) magnetometer. Heat capacity and standard four-probe ac ($f=16$ Hz) resistivity in zero field and applied field of up to 140 kOe were measured in a Quantum Design PPMS-14 instrument using a ^{3}He refrigerator with heat capacity and ac transport options, respectively. In all measurements an external field was applied along the easy magnetic axis ($H \| b$).[13] Resistivity in applied field was measured in a transverse, $H \perp I$, configuration.

The low-field magnetic susceptibility, $\chi = M/H$, measurements and 2 K magnetization, $M(H)$, isotherms are consistent with the data reported in Ref. 13. The feature associated with the antiferromagnetic transition in χ [or in $d(\chi T)/dT$] (Ref. 14) shifts to lower temperatures with an increase of the applied magnetic field (Fig. 1). The lower-field metamagnetic transition (Fig. 2) moves to lower fields with an increase of the temperature at which the $M(H)$ data were taken. At higher temperatures, a second feature moves to an accessible field range (upper left inset to Fig. 2); this feature corresponds to the high-field break in $M(H)$ slope reported previously.[13]

Field-dependent resistivity isotherms are shown in Fig. 3. Two features (marked with dashed lines), consistent with those seen in the aforementioned magnetization [$M(H)$] measurements, are easily recognizable and can be monitored in the H-T domain of the experiments. The position of the lower-field feature is almost temperature independent, while the critical field associated with the higher-field feature decreases with an increase of temperature.

Representative temperature-dependent resistivity, $\rho(T)$, curves are shown in Fig. 4. No traces of the signal from residual Sn flux are seen in $H=0$ data. The resistivity at the base temperature, $T \approx 400$ mK, in zero field is ≈ 2 $\mu\Omega$ cm, consistent with $\rho_0 = 1.5$ $\mu\Omega$ cm obtained from the $\rho = \rho_0 + AT^2$ fit in Ref. 13. A clear break of the $\rho(T)$ slope and the lower-temperature decrease of resistivity below the magnetic

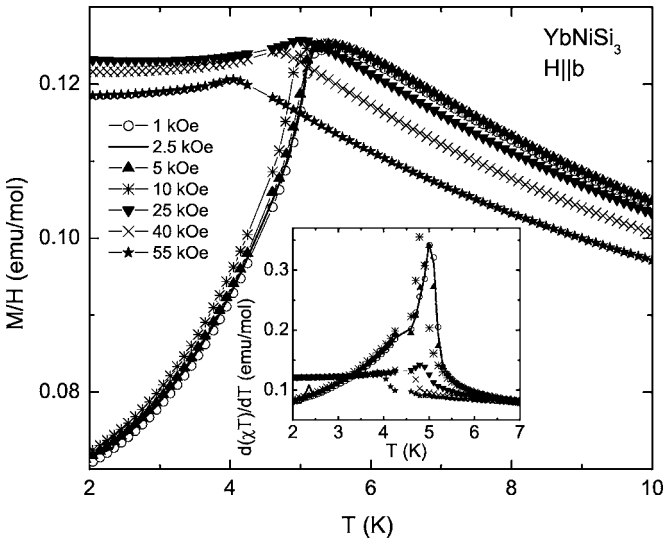

FIG. 1. Low-temperature dc magnetic susceptibility, $M(T)/H$, measured in $YbNiSi_3$ in different applied fields, $H\|b$. Inset: $d(\chi T)/dT$ corresponding to the data in the main panel. Gap in the data near between 4.3 and 4.6 K corresponds to the region of unstable temperature control in our MPMS-5 magnetometer.

ordering temperature T_N associated with a loss of spin-disorder scattering is observed up to 70 kOe. At higher fields, no signature of a magnetic transition can be seen. Moreover, there in no clear signature of the traditional form of non-Fermi-liquid behavior (linear or close-to-linear temperature dependence of resistivity) at fields close to the one for which T_N is suppressed to $T=0$ (Fig. 4, inset).

The temperature-dependent heat capacity is shown in Fig. 5. Results in zero field are consistent with the published data.[13] Consistent with the aforesaid, the peak in $C_p(T)$ moves down with an increase of the applied magnetic field,

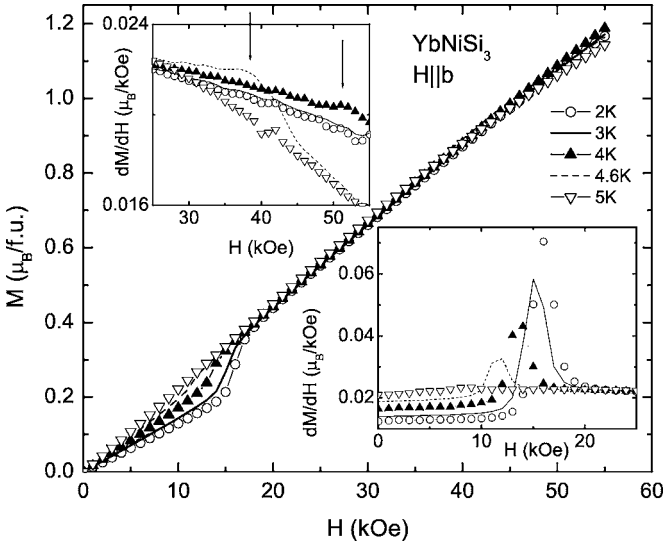

FIG. 2. Representative magnetic isotherms, $M(H)$, measured in $YbNiSi_3$ at different temperatures for $H\|b$. Insets: enlarged low- and high-field plots of corresponding dM/dH. Arrows on the upper left inset mark the second high-field feature, which broadens beyond the resolution for $T=5$ K.

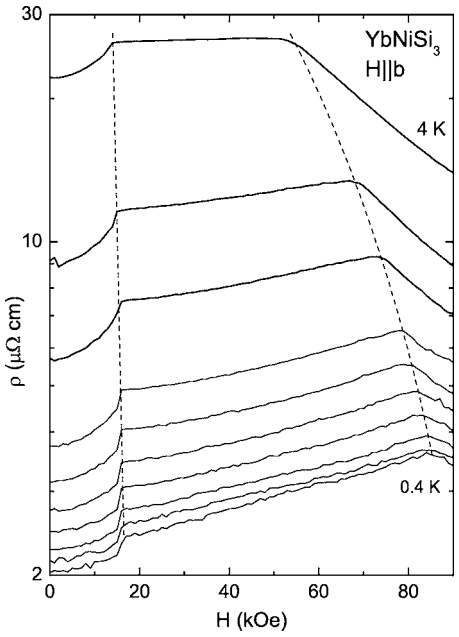

FIG. 3. Low-temperature resistivity isotherms, $\rho(H)$, measured at (from the bottom to the top) 0.4, 0.76, 1, 1.25, 1.5, 1.75, 2, 2.5, 3, and 4 K. Dashed lines are guide for the eye.

its height decreases, and it is no longer detectable in the data at 80 kOe and above. A closer examination of the $H=70$ kOe curve [Fig. 5(b)] reveals that the peak associated with the magnetic long-range order is located on a background with a broad maximum. It is seen with more clarity if C_p/T is plotted as a function of temperature [inset of Fig. 5(b)]. This broad maximum moves up in temperature and acquires structure with an increase of applied field: the data for $H=120$ and 140 kOe can be deconvoluted to up to three

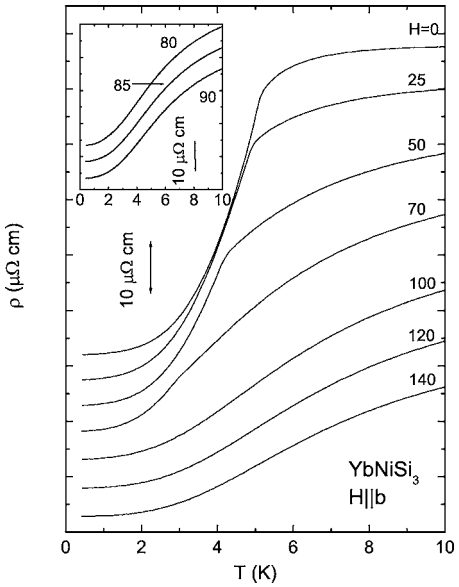

FIG. 4. Representative low-temperature resistivity curves measured in zero and applied magnetic fields. Curves are shifted down along the Y axis by multiples of 5 $\mu\Omega$ cm for clarity. Numbers correspond to the applied field in kOe.

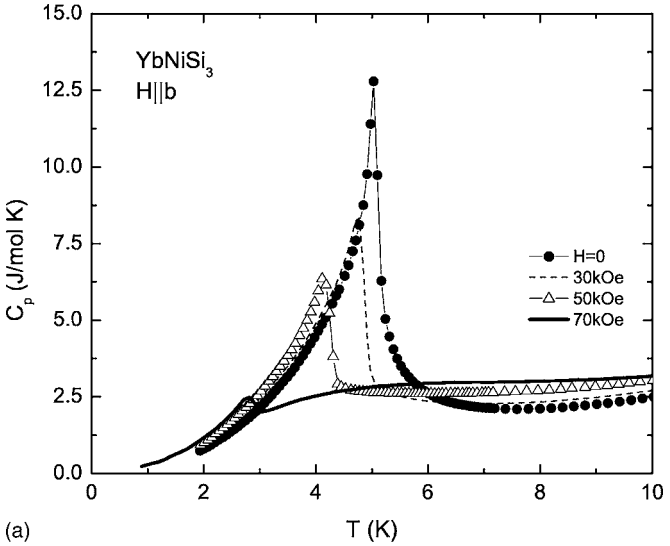

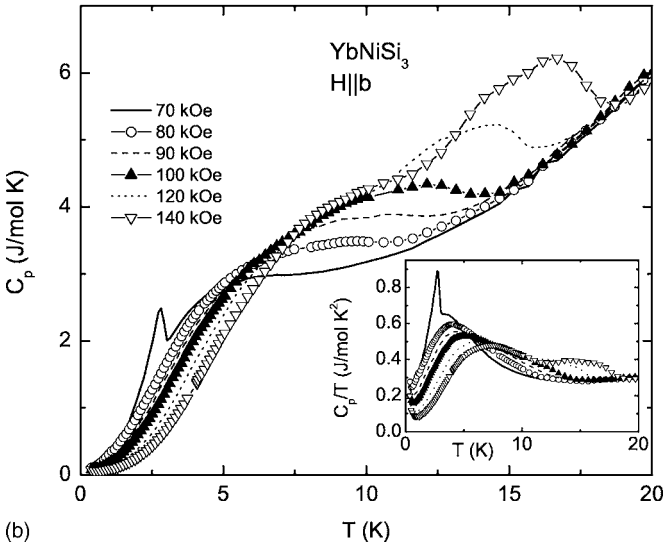

FIG. 5. Low-temperature heat capacity, $C_p(T)$, measured in different applied magnetic fields. Inset of panel (b): C_p/T as a function of temperature. Note that the curve for $H=70$ kOe is shown on both panels.

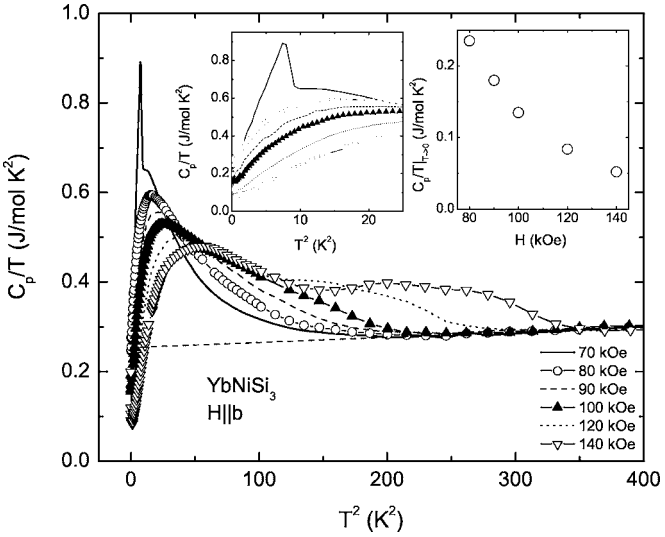

FIG. 6. Heat capacity in applied field for $70 \leqslant H \leqslant 140$ kOe plotted as C_p/T vs T^2. Dashed line—linear extrapolation from the high-temperature data. Insets: left—enlarged low-temperature part and right—estimate of γ from the extrapolated low-temperature linear portion of the C_p/T vs T^2 graph.

broad peaks. For $H \leqslant 50$ kOe, this broad nonmonotonic background is probably obscured by the feature in $C_p(T)$ associated with the magnetic transition. The plausible explanation for these broad features is that they are Schottky-type contributions to the specific heat: the degeneracy of the crystal-electric-field-defined lower-energy levels of $YbNiSi_3$ (e.g., two closely spaced doublets) is lifted by the Zeeman term of the Hamiltonian, and the energy difference between different levels increases further on increase of the applied field. This scenario is in dispute with the assumption of the doublet ground state of $YbNiSi_3$ (Ref. 13) and calls for additional studies.

In order to evaluate the change of the electronic specific heat coefficient γ, the heat capacity data are replotted as C_p/T vs T^2 in Fig. 6. The small upturn at low temperatures (left inset of Fig. 6) that becomes more pronounced at higher fields is probably associated with the nuclear Schottky contribution to the specific heat. The Sommerfeld coefficient in the specific heat, γ, can be estimated by extrapolating the high-temperature linear part of the C_p/T vs T^2 curves to $T=0$ (dashed line in Fig. 6). As a result of such procedure, $\gamma \approx 250$ mJ/mol K^2, practically independent of the applied field, can be assessed. This value is close to the estimate in Ref. 13 for $H=0$. However, this estimate exceeds significantly the values of C_p/T measured in $T \to 0$ regime for magnetic fields in which the magnetic order is suppressed, pointing out that, at least for $70 \leqslant H \leqslant 140$ kOe, high-temperature extrapolation of C_p/T vs T^2 is not a unique estimate of γ. This brings back the question of the estimate of the entropy associated with the magnetic transition[13] and may point out that (in lieu of the data on a nonmagnetic analog) the nonmagnetic contribution, taken as extrapolation from above 10 K, was overestimated, and the cited value of $\Delta S_{mag} \sim 0.6R \ln 2$ was underestimated.

Operationally, one can take the extrapolation to $T \to 0$ of the lowest-temperature measurements plotted as C_p/T vs T^2 (see left inset of Fig. 6) (ignoring the nuclear Schottky contribution), as an estimate of γ. The obtained values (right inset of Fig. 6) seem to follow the trend generally observed in materials close to a QCP.[10–12,15,16] However, at least in the particular case of $YbNiSi_3$, one cannot discard the possibility that the shifts of the Schottky-type peaks to higher temperatures with the increasing applied field lead to a decreasing contribution (since it is taken further from the maximum) to the apparent $\gamma = C_p/T|_{T \to 0}$, and the genuine behavior of the Sommerfeld coefficient is masked by this fast changing contribution.

The thermodynamic and transport measurements performed on $YbNiSi_3$ with the magnetic field applied along the b axis define the H-T phase diagram (Fig. 7). This phase diagram is consistent (in overlapping H-T domains) with the one recently suggested[17] from magnetoresistance isotherms

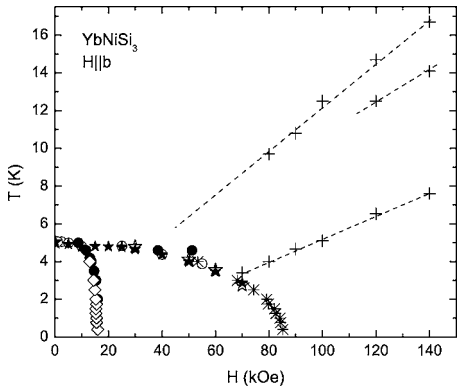

FIG. 7. *H-T* phase diagram of $YbNiSi_3$ for $H \| b$. Different symbols correspond to the phase lines obtained from different thermodynamic and transport measurements: open circle—$M(T)$, filled circle—$M(H)$, open star—$C_p(T)$, filled star—$\rho(T)$, and diamond and asterisk—$\rho(H)$. Crosses correspond to the position of broad maxima in C_p/T and dashed lines are guides for the eye.

for $T \geqslant 1.85$ K. The phase diagram is rather simple, with only two phases in the ordered state and a triple point. The positions of the Schottky-type anomalies are also shown; depending on the applied field in a close to linear fashion. A magnetic field of ~85 kOe suppresses the phase transition we assume to be associated with long-range magnetic order, making the phase diagram look similar to the cases of field-induced QCP recently discussed in several materials.[10–12,15,16]

Further understanding of the low-temperature state of $YbNiSi_3$ in applied field can be approached by a detailed analysis of the magnetotransport and thermodynamic data. Low-temperature resistivity $[\rho(T)]$ data measured in magnetic field were fitted with the equation $\rho(T)=\rho_0+AT^{\beta}$ (e.g., as in Ref. 18) with three fitting parameters: residual resistivity ρ_0, prefactor A, and exponent β. Two sets of fits were performed: from 3 K down to the base temperature (≈0.4 K) and from 1.5 K down to the base temperature. Both sets of fits give similar results (Fig. 8). All three fitting parameters have features associated with the critical fields, the lower critical field being essentially temperature independent below 3 K and the upper one only shifting slightly as T decreases from 3 to 1.5 K (as can be seen in A and β). It is noteworthy that the exponent β as calculated from the data above ≈0.4 K does not fall below $\beta=2$, and the changes in β as obtained from the $0.4 \geqslant T \geqslant 1.5$ K are rather small (Fig. 8, upper panel). This is clearly distinct from the case of field-induced QCP in $YbRh_2Si_2$,[10,15] YbAgGe,[11,18] and other materials, although it is possible that β may approach 1.0 for $T<0.4$ K and in a very narrow field range. These different functional behaviors of resistivity and specific heat in $YbNiSi_3$ near the critical field may be caused by the additional contributions from the Schottky-type anomalies from the magnetic-field-split low-lying energy levels that are more

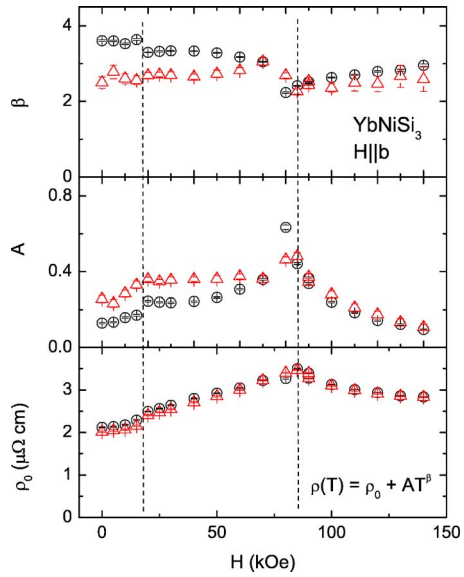

FIG. 8. (Color online) Results of fitting of low-temperature resistivity to the form $\rho(T)=\rho_0+AT^{\beta}$; units of $\rho(T)$ and ρ_0 are in $\mu\Omega$ cm. Circles: fit from 3 K to the base temperature and triangles: fit from 1.5 K to the base temperature. *Nominal* error bars of the fits are shown. Vertical dashed lines mark $T \to 0$ critical fields from the phase diagram above.

susceptible to the applied field than in $YbRh_2Si_2$ or YbAgGe.

In summary, thermodynamic and transport measurements on $YbNiSi_3$ ($H \| b$) reveal an *H-T* phase diagram with two distinct magnetically ordered phases and a triple point. An applied magnetic field of ~85 kOe suppresses the magnetic ordering temperature. Unlike several known heavy fermions with field-induced QCP, above 400 mK no non-Fermi-liquidlike signature in the resistivity data was observed in the vicinity of the critical field for $T \geqslant 0.4$ K, although they may well emerge for $T<0.4$ K data. Heat capacity measurements suggest that the applied magnetic field splits the nearly degenerate levels that form the zero-field ground state of $YbNiSi_3$, and this field-dependent split of the energy levels manifests itself as Schottky-type anomalies.

ACKNOWLEDGMENTS

Ames Laboratory is operated for the U.S. Department of Energy by Iowa State University under Contract No. W-7405-Eng.-82. Work at Ames Laboratory was supported by the Director for Energy Research, Office of Basic Energy Sciences. Work in Hiroshima University was supported by a Grant-in-Aid for Scientific Research (COE Research 13CE2002) of MEXT Japan. P.C.C. acknowledges R. A. Ribeiro for having devised the three-finger method of small sample manipulation. S.L.B. and M.A.A. acknowledge the help of Kamotsuru in the initial stage of this work.

[1] R. B. Laughlin, G. G. Lonzarich, P. Monthoux, and D. Pines, Adv. Phys. **50**, 361 (2001).
[2] G. R. Stewart, Rev. Mod. Phys. **73**, 797 (2001).
[3] G. R. Stewart, Rev. Mod. Phys. **78**, 743 (2006).
[4] P. Coleman, C. Pépin, Q. Si, and R. Ramazashvili, J. Phys.: Condens. Matter **13**, R723 (2001).
[5] S. Sachdev, Science **288**, 475 (2000).
[6] P. Gegenwart, J. Custers, T. Tayama, K. Tenya, C. Geibel, G. Sparn, N. Harrison, P. Kerschl, D. Eckert, K.-H. Müller *et al.*, J. Low Temp. Phys. **133**, 3 (2003).
[7] M. A. Continentino, Braz. J. Phys. **35**, 1 (2005).
[8] P. Coleman and A. J. Schofield, Nature (London) **433**, 226 (2005).
[9] S. Doniach, in *Valence Instabilities and Related Narrow-Band Phenomena*, edited by R. D. Parks (Plenum, New York, 1977), p. 169.
[10] P. Gegenwart, J. Custers, C. Geibel, K. Neumaier, T. Tayama, K. Tenya, O. Trovarelli, and F. Steglich, Phys. Rev. Lett. **89**, 056402 (2002).
[11] S. L. Bud'ko, E. Morosan, and P. C. Canfield, Phys. Rev. B **69**, 014415 (2004).
[12] E. Morosan, S. L. Bud'ko, Y. A. Mozharivskyj, and P. C. Canfield, Phys. Rev. B **73**, 174432 (2006).
[13] M. A. Avila, M. Sera, and T. Takabatake, Phys. Rev. B **70**, 100409(R) (2004).
[14] M. E. Fisher, Philos. Mag. **7**, 1731 (1962).
[15] J. Custers, P. Gegenwart, H. Wilhelm, K. Neumaier, Y. Tokiwa, O. Trovarelli, C. Geibel, F. Steglich, C. Pépin, and P. Coleman, Nature (London) **424**, 524 (2003).
[16] L. Balicas, S. Nakatsuji, H. Lee, P. Schlottmann, T. P. Murphy, and Z. Fisk, Phys. Rev. B **72**, 064422 (2005).
[17] K. Grube, T. Wolf, P. Adelmann, C. Meingastand, and H. von Löhneysen, Physica B **378-380**, 750 (2006).
[18] P. G. Niklowitz, G. Knebel, J. Flouquet, S. L. Bud'ko, and P. C. Canfield, Phys. Rev. B **73**, 125101 (2006).